Journal of Molecular Catalysis B: Enzymatic 69 (2011) 1–7

Contents lists available at ScienceDirect

Journal of Molecular Catalysis B: Enzymatic

journal homepage: www.elsevier.com/locate/molcatb

Glucose biosensor based on the highly efficient immobilization of glucose oxidase on Prussian blue-gold nanocomposite films

Chengyan Wang, Shihong Chen*, Yun Xiang, Wenjuan Li, Xia Zhong, Xin Che, Jingjing Li

Key Laboratory of Chongqing Modern Analytical Chemistry, Education Ministry Key Laboratory on Luminescence and Real-Time Analysis, College of Chemistry and Chemical Engineering, Southwest University, Chongqing 400715,China

ARTICLE INFO

Article history:
Received 10 July 2010
Received in revised form 6 December 2010
Accepted 6 December 2010
Available online 17 December 2010

Keywords:
Biosensor
Prussian blue-gold nanocomposite
Platinum nanoclusters
Glucose oxidase
Electrochemical deposition

ABSTRACT

A glucose biosensor was developed, which was based on Prussian blue-gold (PB-Au) nanocomposite films and platinum nanoclusters (Pt-NCs). Prussian blue (PB), as an electron mediator, was electrochemically deposited on the glass carbon electrode (GCE) in the presence of chloroauric acid, forming PB-Au nanocomposite films. Then, Pt-NCs were electrodeposited to construct a bilayer film. At last, glucose oxidase was modified on the electrode with the bilayer film and the film of Nafion (Nf) was used to prevent the glucose oxidase (GOD) from leaking off. The resulting amperometric glucose biosensor exhibited a fast response time (within 8 s) and a linear calibration range from 3.0 μM to 1.1 mM with a low detection limit of 1.0 μM glucose (S/N = 3). With the low operating potential, the biosensor showed little interference to the possible interferents, including acetum acid, uric acid and arginine, indicating an excellent selectivity. The improved performances of resulting electrode for electrocatalysis-oxidation glucose were ascribed to the high surface-to-volume ratio and the excellent catalytic activity of nanoparticles. The combination of the PB-Au nanocomposite and Pt-NCs would open new horizons for fabrication of biosensors and biocatalysts.

1. Introduction

Recently, tremendous attention has been paid to the nanoscale materials due to their unique physicochemical characteristics, such as the catalytic activities, optical properties, electronic properties and magnetic properties that cannot be achieved by their bulk counterparts [1]. The nanostructured materials have a broad range of potential importance to analysis and catalysis [2,3]. To construct a biosensor with good performance, the immobilization of the biomolecule is great pivotal. Fortunately, the conductive nanometer scale structures with good stability and highly catalytic ability favor to the immobilization of the biomolecule and can enormously improve the performance of biosensors [4]. The nanostructured materials, such as metal [5], metal oxide [6], alloy [7], carbon nanotube [8], have been extensively applied in the construction of the biosensor at present.

In recent years, noble metal nanoparticles have been extensively utilized owing to their extraordinary catalytic activities [9–12]. Particularly, Pt nanoparticles have attracted a substantive research subject for the fabrication of electrodes [13–15]. For example, Li et al. [16] decorated the magnetic composite of ferric oxide and multil-wall carbon nanotube (Fe_xO_y–MWCNTs) with Pt nanoparticles to construct an amperometric glucose biosensor. The combination of Fe_xO_y–MWCNTs and Pt nanoparticles in the biosensor results in a linear range and a lower detection limit for glucose determination, as compared to those MWCNTs and Fe_xO_y-based glucose biosensors. Catalytic activity is one of the most important properties of Pt nanoparticles. Compared with the Pt nanoparticles, platinum nanoclusers (Pt-NCs) with a large surface-to-volume ratio can further increase the amount of immobilized enzyme, minimize the barriers for mass transportation between the substrate and the product, and provide a chemically and mechanically robust system. The unique physiochemical properties suggest that Pt-NCs have significantly potential application in chemo/biosensors and catalysts. Li et al. [17] fabricated a nitrite biosensor with PPy–Pt nanocomposite formed by depositing Pt-NCs in polypyrrole (PPy) nanowires, and it performed well with the wide linear calibration range and high sensitivity.

Since 1978 that Neff realized the first study of thin films of Prussian blue (PB) on various metal and semiconductor substrates, PB and several of its analogues have been of significant interest in many different research areas [18]. The ferriferrocyanide complex PB is electrochemically reduced to form Prussian white (PW), which is capable of catalysing the reduction of hydrogen peroxide (H_2O_2) at low potentials like peroxidases, so it is referred to as "artificial peroxidase" [18,19]. The detection mode involved in

* Corresponding author. Tel.: +86 23 68253172; fax: +86 23 68253172.
E-mail address: cshong@swu.edu.cn (S. Chen).

1381-1177/$ – see front matter © 2010 Elsevier B.V. All rights reserved.
doi:10.1016/j.molcatb.2010.12.002

oxidase-based biosensors is often based on the electrochemical detection of H_2O_2, which is produced during the enzyme-catalyzed oxidation of substrates by dissolved oxygen [20]. In the same way, most amperometric glucose biosensors are determining the enzymatically liberated H_2O_2 by electrochemical methods. The glucose biosensors constructed with PB [21–23] exhibit the short response time and high electrocatalytic activity and sensitivity of electrochemical response to glucose, and show a significantly decreased background, resulting in improved signal-to-noise ratio. However, the lower electrochemical stability of the PB films and the subsequently lower operational stability of the PB-based biosensors at near neutral solution [24,25] seriously restrain the further development of this kind of biosensors, because the oxidase enzymes which produce H_2O_2 in an enzyme-catalyzed reaction usually are operated at near neutral solution. To resolve this problem, several measures have been adopted, including reducing the pH of the buffer solutions [26], synthesizing PB nanoparticles [4], wrapping PB around the organic substances [23] or depositing it with other materials to obtain composites [27].

Kumar et al. [28] reported the one-step electrochemical deposition of PB-Au nanocomposite films and developed a H_2O_2 biosensor. Ahmadalinezhad et al. [22] developed a glucose biosensor, which was based on the immobilization of glucose oxidase (GOD) on a PB modified nanoporous gold surface. In this study, we reported a glucose biosensor based on Pt-NCs and PB-Au films formed by the way of one-step electrochemical deposition. The biosensor prepared by the method can be operated at a low potential with a broad linear range, low detection limit, short response time and high sensitivity. Compared with those systems based on the enzyme immobilized onto the films of the pure PB nano-particulates directly [29–31], our presented system based on PB-Au/Pt-NCs matrix possesses superior performance because of following reasons. Firstly, the nanocomposite of PB and nano-Au provided two merits for the glucose biosensor. On the one hand, the forming of PB-Au nanocomposite is in favor of the immobility of the electron mediator PB, alleviating the problem of the stability of PB, which is mentioned in the reference [24,25]. On the other hand, nano-Au, as a popular noble metal, owing the satisfactory conductivity, can transmit the electrons rapidly and provide a favorable microenvironment for retaining biological activity of enzymes. Secondly, with a large surface-to-volume ratio of the Pt-NCs, more GOD could be immobilized tightly on the films of PB-Au/Pt-NCs. Moreover, the Pt-NCs are capable of catalyzing the reduction of H_2O_2 intrinsically. Consequently, both PB-Au nanocomposites and Pt-NCs are the outstanding matrixes for the construction of glucose biosensor. Such a fabrication technology demonstrated in this paper brings a new platform for electrochemical biosensor by using the synergistic effect of the electrocatalytic activity of PB-Au and Pt-NCs.

2. Experimental

2.1. Materials

Glucose oxidase (GOD), Nafion (Nf), chloroplatinic acid ($H_2PtCl_6{\cdot}6H_2O$) and chlorauric acid ($HAuCl_4{\cdot}4H_2O$) were purchased (Sigma, St. Louis, MO, USA). Potassium ferricyanide ($K_3[Fe(CN)_6]$), Potassium nitride (KNO_3), nitric acid (HNO_3), Potassium hydroxide (KOH) and Ethylene glycol ($C_2H_6O_2$) were obtained (Chongqing Chuandong Chemical Regent Co., Chongqing, China). All other chemicals were of analytical grade and used without further purification. Double-distilled water was used throughout this study. A stock solution of 2.0 mg/ml GOD was freshly prepared with 0.1 M phosphate buffer solution (pH 6.5).

2.2. Apparatus and measurements

Electrochemical impedance spectroscopy measurements were carried out with a Model IM6e (ZAHNER Elektrick Co., Germany) in the presence of a 5.0 mM $K_3[Fe(CN)_6]/K_4[Fe(CN)_6]$ (1:1) mixture as a redox probe. The alternative voltage was 5 mV and the frequency range was 50 mHz–10 kHz. Transmission electron microscopy (TEM) was performed on a TECNAI 10 (PHILIPS FEI Co., The Netherlands). Atomic force microscopy (AFM) images of the films were achieved by scanning probe microscope (SPM) (Vecco, USA). Amperometric experiments and cyclic voltammetric experiments were performed using a CHI 660A electrochemical work station (Shanghai CH Instruments Co., China) in a three-electrode electrochemical cell containing a platinum wire auxiliary electrode, a modified GCE as working electrode and a saturated calomel electrode (SCE) as reference electrode against which all potentials were measured. The test solutions were potassium nitrate buffer solutions. All the electrochemical experiments were carried out at room temperament.

2.3. Glucose biosensor fabrication

2.3.1. Preparation of Pt-NCs

Pt-NCs were prepared according to the procedure described in the literature [32]. All operations were carried out under inert atmosphere (N_2). Typically, 50 ml Ethylene glycol solution of NaOH (0.5 mol/l) was added into 50 ml Ethylene glycol solution of $H_2PtCl_6{\cdot}6H_2O$ (1.93 mmol/l) with stirring to obtain a yellow platinum hydroxide or oxide colloidal solution which was then heated at 160 °C for 3 h, with N_2 slowly passing through the reaction system to take away water and organic byproducts. A transparent dark-brown homogeneous colloidal solution of the Pt-NCs (Pt: 3.76 g/l Ethylene glycol, 19.3 mmol/l) was obtained without any precipitate. The obtained Pt-NCs solution was very stable, no precipitate had been observed several months later.

2.3.2. Modification of the electrode

The glass carbon electrode (Φ = 4 mm) (GCE) was used for the glucose biosensor. The electrode was carefully polished with alumina slurry (grain size, 0.3 mm and 0.05 mm) until a mirror was obtained. Ultrasonic rinsing with ethanol and water was necessary to remove the alumina residues from the electrode surface. Such prepared electrode was dried. For the growth of PB-Au films, a solution of 0.1 M KNO_3 at pH 3.2 containing equimolar (1 mM) potassium ferricyanide and chloroauric acid was employed [28]. And the range of the depositing potential was from 0.0 V to 1.0 V. The films formed after 20 potential cycles between 0.0 V and 1.0 V was examined for their cyclic voltammetric behavior in a blank solution of 0.1 M KNO_3. After the solvent evaporating, Pt-NCs were deposited on the PB-Au composite films under the potential of −0.25 V for 120 s and dried in air. The construction of the enzyme electrode was accomplished as follows: 10 μl GOD (2 mg/ml) was modified onto the Pt-NCs/PB-Au/GCE. After drying in refrigerate, the electrode was coated by 5 μl of Nafion (0.5 wt%) to stabilize the adherence of the modified layer and dried at 4 °C. The procedure for preparing glucose biosensor is schematically shown in Scheme 1. As the control experiment, Nf/GOD/PB-Au/GCE was fabricated using the same procedure as described above except that Pt-NCs were not involved.

3. Results and discussion

3.1. The response mechanism of the biosensor

The mechanism involve in the detection of glucose with generation of H_2O_2 is the same as the literature [33–35]. GOD catalyzes the

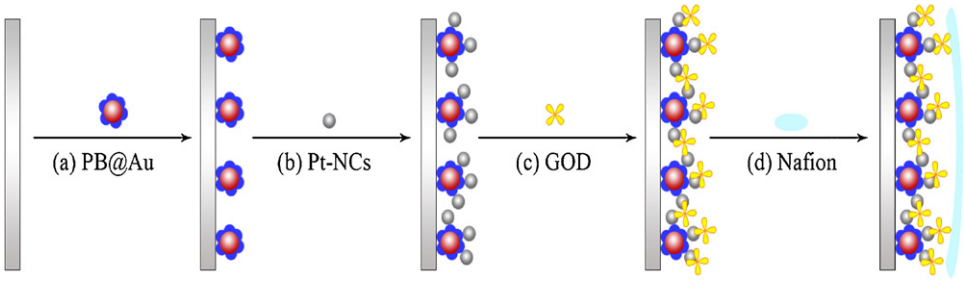

Scheme 1. The illustration of the preparation process of modified electrode.

oxidation of glucose in the presence of molecular oxygen according to Eqs. (1) and (2), producing H_2O_2, so the concentration of H_2O_2 is directly proportional to the concentration of the glucose. Therefore, the concentration of the glucose can be monitored indirectly during the course of the reaction.

$$\text{GOD(FAD)} + \beta\text{-D-glucose} \rightarrow \text{GOD(FADH}_2\text{)} + \beta\text{-D-gluconolactone} \quad (1)$$

$$\text{GOD(FADH}_2\text{)} + O_2 \rightarrow \text{GOD(FAD)} + H_2O_2 \quad (2)$$

PB films can be reduced to the colorless form PW, as shown in Eq. (3): where Fe^{II} and Fe^{III} correspond to different oxidation states of Fe atoms in the PB structure. PW can electrocatalytically reduce H_2O_2, acting as an electron transfer mediator between the substrate and H_2O_2 formed in the enzymatic reaction. Here we employed a PB-Au layer obtained via one-step electrochemical deposition, which has been proven to yield stable films with good electrocatalytic properties for reduction of H_2O_2 [26].

$$K_2Fe^{2+}Fe^{2+}(CN)_6(PW) \overset{H_2O_2}{\underset{e}{\rightleftharpoons}} KFe^{3+}Fe^{2+}(CN)_6(PB) + K^+ \quad (3)$$

3.2. The characterization and electrochemical measurements of the biosensor

3.2.1. TEM of the Pt-NCs

TEM was employed to characterize the shape and size of the synthesized Pt-NCs. The TEM image of Pt-NCs shows the presence of spherical nanoparticles homogeneously dispersed in Ethylene glycol (Fig. 1). It is obviously that no particle agglomeration appeared, suggesting that Ethylene glycol stabilized the Pt-NCs and prevented the further aggregation of the particles. The nanoclusters have an average particle size of about 4.6 nm and a size distribution from 3 to 6 nm.

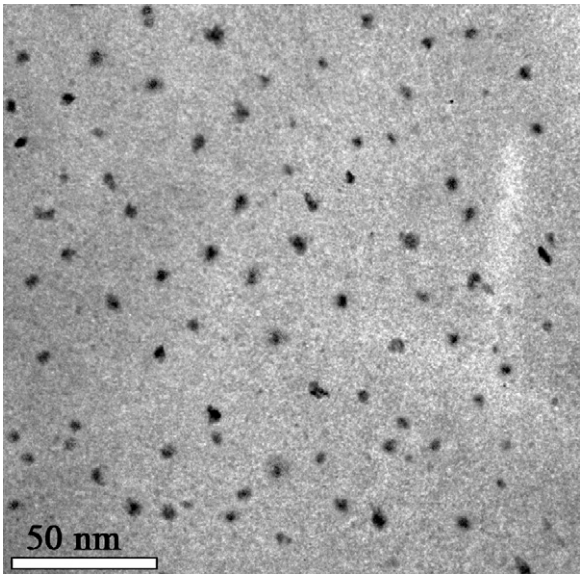

Fig. 1. TEM image of platinum nanoclusters.

3.2.2. Atomic force microscopy (AFM)

Fig. 2 shows the surface to topographic images of films of the stepwise biosensor fabrication process using the AFM technique with tapping mode. As can be seen from Fig. 2a, PB-Au nanocomposite aggregates were observed from the films formed using $K_3[Fe(CN)_6]$ and $HAuCl_4$. It was convinced that the gold nanoparticles being the "seeds" for the growth of PB were hidden inside of the aggregates [28]. And the globular particles with the small size are the unmodified exposed gold nanoparticles formed during the deposition cycles. When Pt-NCs grows on films of the PB-Au surface, the topographies image is similar to that of PB-Au nanocomposite, which may be attribute to the small size and the pattern of the Pt-NCs as similar as that of the gold nanoparticles and the PB-Au nanocomposite aggregates (Fig. 2b). Then the assembly of GOD on the films of Pt-NCs/PB-Au surface is observed from Fig. 2c. The phase figure part in the AFM image of GOD/Pt-NCs/PB-Au films exhibited a smoothing effect as compared to that of Pt-NCs/PB-Au films, which might be due to GOD molecules filling the interstitial places between PB-Au nanocomposites and Pt-NCs.

3.2.3. EIS and CV characterization

It is well known that EIS is an alternative powerful tool for measuring the changes of interface properties on the modified electrode surfaces. In order to acquire more information from EIS results, the working electrode was modeled with an equivalent circuit (inset of Fig. 3A). The equivalent circuit consists of an electrolyte solution resistance R_s, a parallel double layer capacitance C_{dl}, electron-transfer resistance R_{et} and the Warburg impedance Z_w. Depending on the dielectric and insulating features on the electrode/electrolyte interface, the combination of R_{et} and C_{dl} bring about a semicircle in the Nyquist plot (Z'' vs. Z'). By the means of measuring the diameter of the semicircle in the impedance spectrum via simulation, the electron-transfer resistance R_{et} can be obtained. The electrochemical impedance studies of the modified electrodes were performed and the results are shown in Fig. 3A. The curve a (Fig. 3A) shows EIS of the bare GCE. There is a small semicircle at high frequencies and a linear part at low frequencies, as was reported, implying low R_{et} ($R_{et} = 134\,\Omega$) to the redox probe dissolved in the electrolyte solution. A decrement of resistance was observed at the PB-Au/GCE (curve b), in contrast to the resistance of the bare GCE, which proves that PB-Au nanocomposite is beneficial to the electron transfer. When Pt-NCs were deposited onto PB-Au films, a further decrease of R_{et} is observed (curve c), which is on account of the favorable conductive property of Pt-NCs. Compared with the Pt-NCs/PB-Au/GCE, the EIS of the Nf/GOD/Pt-NCs/PB-Au/GCE presents an obvious increase in R_{et} ($R_{et} = 513\,\Omega$, curve d), suggesting that GOD and Nf were successfully assembled on the surface of the resulting electrode. This increase is due to the

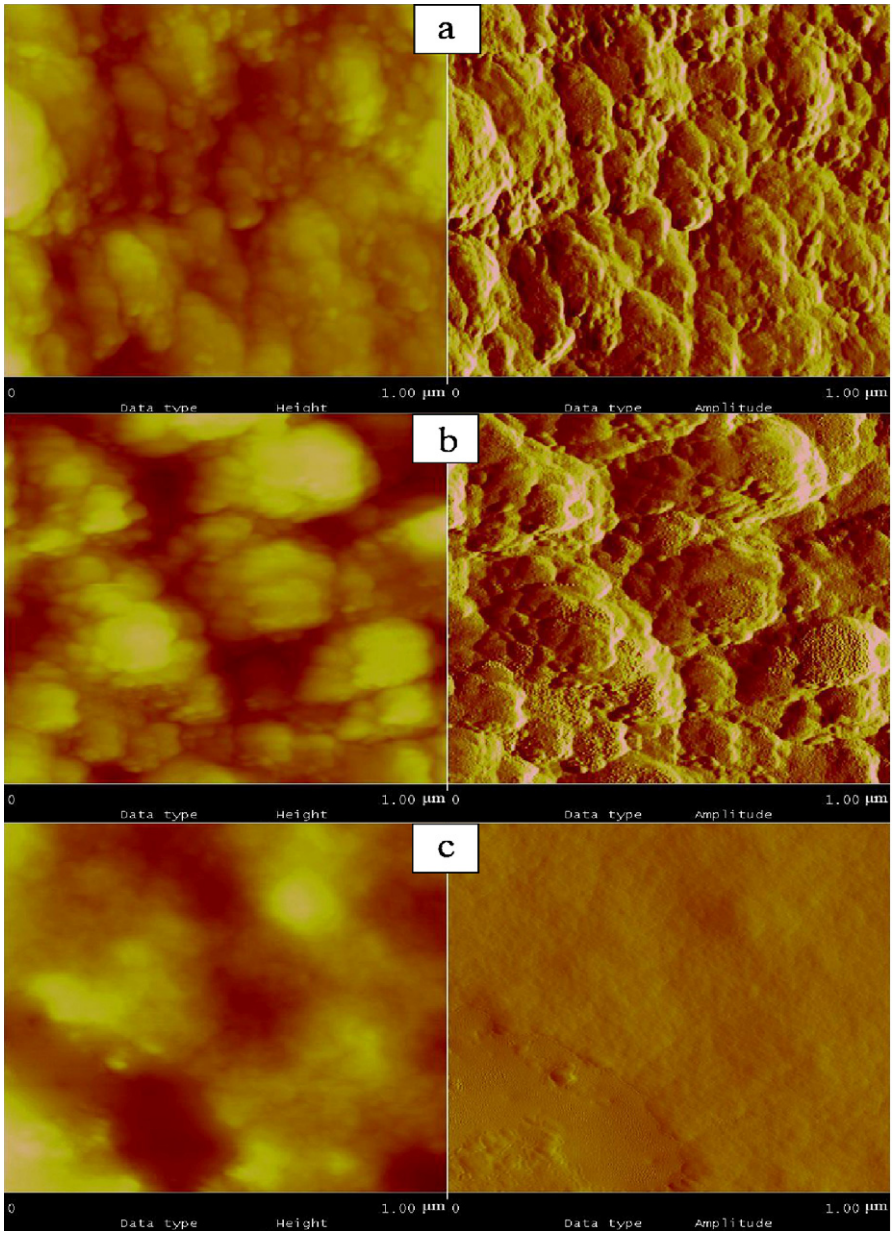

Fig. 2. AFM images of PB-Au composite films (a), Pt-NCs/PB-Au films (b) and GOD/Pt-NCs/PB-Au films (c) on the gold surface.

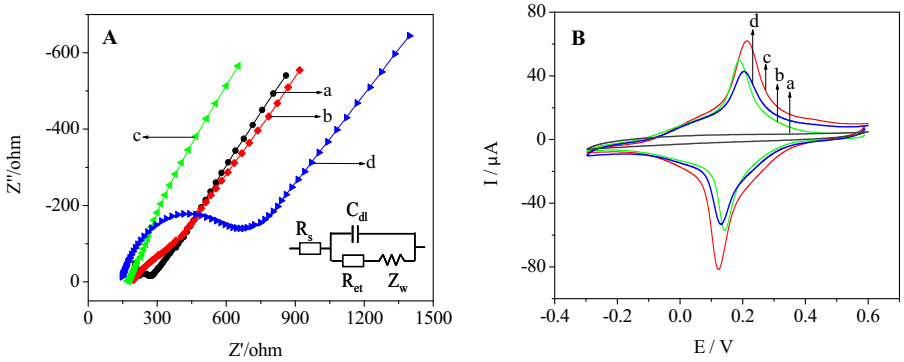

Fig. 3. (A): EIS of bare GCE (a), PB-Au/GCE (b), Pt-NCs/PB-Au/GCE (c) and Nf/GOD/Pt-NCs/PB-Au/GCE (d) in 5.0 mM $K_3[Fe(CN)_6]/K_4[Fe(CN)_6]$ (1:1); Inset: equivalent circuit used to model impedance data. (B) Cyclic voltammograms obtained at a scan rate of 50 mV/s from different modified electrodes in 0.1 M KNO_3 (pH 6.0) solution. The bare GCE (a), PB-Au/GCE (b), Pt-NCs/PB-Au/GCE (c), and Nf/GOD/Pt-NCs/PB-Au/GCE (d).

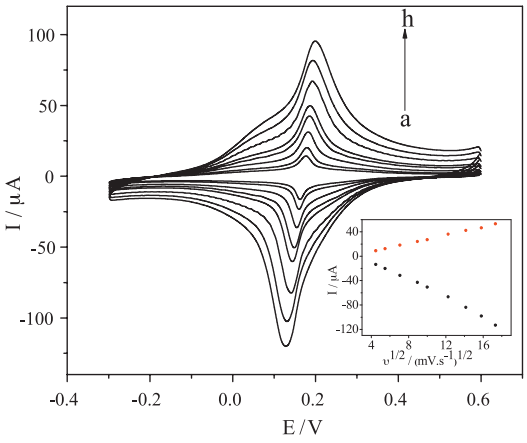

Fig. 4. The cyclic voltammograms of Nf/GOD/Pt-NCs/PB-Au/GCE in 0.1 M, pH 6.0, KNO_3 solution at various scan rates. From curves a to h corresponding to 30, 50, 80, 100, 150, 200, 250, 300 mV/s. Inset: The relationship between the peak currents and scan rates.

non-conductive properties of GOD and Nf films. The impedance change obtained after the modification process proves that PB-Au, Pt-NCs, GOD and Nf had been successively assembled on the surface of the GCE.

Fig. 3B displays the cyclic voltammograms (CVs) at differently modified electrodes in 0.1 M KNO_3 (pH 6.0) solution. The curve a (Fig. 3B) is the CVs obtained at a bare GCE in KNO_3. No obvious electrochemical peak in this potential range was observed as the lack of electron mediator. In contrast, after the PB-Au composite was deposited on the electrode, a pair of well-defined peaks can be observed (curve b), characteristic of PB redox couple. In comparison with it, the peak currents increase after Pt-NCs modification (curve c in Fig. 3B). Apparently, the presence of the Pt-NCs is an essential component for the electron transfer. The reason is that nanometer-sized particle play an important role, similarly to a conducting wire or electron-conducting tunnel, which enhances the electron-transfer kinetics. With the immobilization of GOD and Nf on the modified electrode surface, an obvious decrease of the peak currents is noted (Fig. 3B curve d). This may be ascribed to the nonconductive property of GOD and Nf, obstructing electron transfer between PB-Au and the surface of the electrode, as observed in EIS.

Fig. 4 shows the CVs of the Nf/GOD/Pt-NCs/PB-Au/GCE recorded in 0.1 M KNO_3 at different scan rates. It is found that both anodic and cathodic peak currents increase clearly with increasing the scan rate. The peak currents are linearly correlated to the square root of the scan rate in the range from 30 mV/s to 250 mV/s (insert of Fig. 4), implying that the electrochemical kinetics is a diffusion-controlled process.

3.3. Optimization of experimental parameters for biosensor

3.3.1. The thickness of the PB-Au film-effect

When the cyclic voltammetric behavior of the GCE on potential cycling between 0.0 V and 1.0 V in 0.1 M KNO_3 medium containing $HAuCl_4$ and $K_3[Fe(CN)_6]$ at the scan rate of 50 mV/s was studied (measured solution pH 3.2), all redox peaks gradually grow and tend to be constant increase with the increase of number of scans (data not shown), which demonstrates that the PB films have formed on the substrate surface. The films' thickness influences the response of the biosensor. A thicker film shows a long response time and a lower sensitivity but result in a wider linear range. Keeping the concentration of $K_3[Fe(CN)_6]$ and $HAuCl_4$ constant (1 mM), the film thickness is easily controlled by limiting the number of scans. In the present experiments, 20 cycles of successive scanning at the scan rate of 50 mV/s was suitable for achieving a higher sensitivity and a relatively wide linearity.

3.3.2. pH-effect and potential-effect

Since the activity of the immobilized GOD and the stability of the PB layer are pH dependent, investigation of the pH value of the detection solution on the performance of the biosensor is of great importance [36]. In the literature [19,20], it is clearly reported that PB is unstable and dissolves at pH values above 7, suggesting a limited use of PB-modified electrodes in alkaline solutions. In this work, Fig. 5A shows the effect of solution pH on the amperometric response at the Nf/GOD/Pt-NCs/PB-Au/GCE. The pH dependence of the enzyme electrode over the pH range 4.0–8.0 in 0.1 M KNO_3 buffer solution in the presence of 60 μM glucose was studied. The optimum response was achieved in the pH 6.0. Therefore, we selected pH 6.0 for this study so as to assure higher sensitivity and the stability of PB.

The choice of the applied potential at the working electrode is fundamental to achieve a low detection limit and to avoid the electrochemical interfering species. So, we also investigated the effect of applied potential on the enzyme electrode response toward constant concentration (60 μM) of the glucose (see Fig. 5B). The results demonstrate that the response currents gradually increase with decreasing negatively applied voltage from 0.2 V to −0.4 V. A more negatively applied voltage would lead to a higher sensitivity, however, it is preferable to control a more positively applied voltage in order to avoid or decrease the interference caused by some coelectroactive species in the sample solution. Hence, a working potential of −0.15 V was chosen for glucose determination in this work, where the biosensor could maintain reasonable sensitivity and avoid the interference caused by some electroactive species.

3.4. The response characteristics of the glucose biosensor

For amperometric biosensing application, electrodes are generally evaluated by measuring current response at a fixed potential with the addition of the analyte in the measuring solution. Fig. 6A illustrates a typical current–time curve of the glucose biosensor upon the addition of different concentration of glucose at −0.15 V in a 0.1 M KNO_3 buffer solution (pH 6.0) under the optimized conditions. The bio-functionality of GOD and the feasibility of the method for biosensing were exhibited by the increase in reduction current upon the addition of successive aliquots of glucose. For Nf/GOD/Pt-NCs/PB-Au/GCE, the 95% of the steady-state current can be obtained within 8 s, which was faster than other glucose biosensors [4,21,33,37]. As can be observed, the glucose biosensor had a fast and sensitive response to the addition of glucose and the glucose biosensor exhibited a wide linearity from 3.0 μM to 1.1 mM. The detection limit of the biosensor is 1.0 μM (S/N = 3) with the sensitivity of 2.77 mA M^{-1}. The wide linear range extended over three orders of magnitude of glucose concentration, indicating that large loading of enzymes was implemented in the immobilization of GOD.

As controlled experiment, the amperometric responses were also measured at the Nf/GOD/PB-Au/GCE. The corresponding typical current–time curves are showed in Fig. 6B. As can be observed, the GOD/PB-Au/GCE showed a relatively small current response to glucose (curve a in Fig. 6B). Such a response was mainly ascribed to the favorable capacity of transferring the electron of PB molecules, which was promoted through the conducting tunnels of nano-Au since they could provide the protein molecules more freedom in orientation. However, with the addition of the glucose, drastic increase in the response current was observed at the Nf/GOD/Pt-NCs/PB-Au/GCE (Fig. 6B curve b). This result demonstrated clearly that the biosensor based on the PB-Au composite and Pt-NCs exhibited a better electro-catalytic activity to glucose due to the

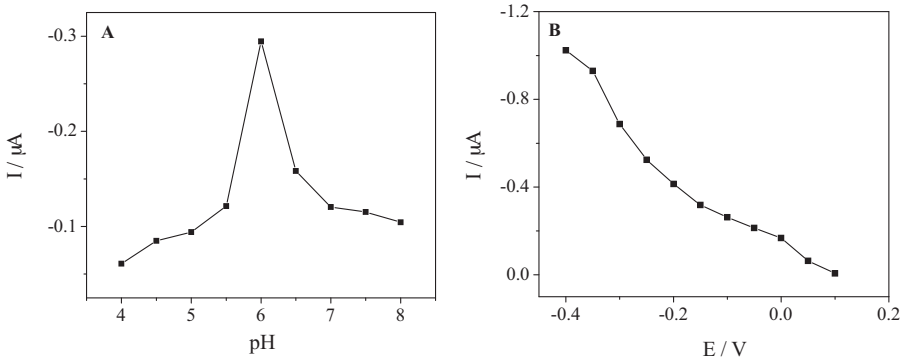

Fig. 5. (A) Dependence of the current response of Nf/GOD/Pt-NCs/PB-Au/GCE to 60 μM glucose on the pH of buffer solutions at an applied potential of −0.15 V. (B) Dependence of the current response of the Nf/GOD/Pt-NCs/PB-Au/GCE to 60 μM glucose on the applied potential in 0.1 M KNO_3 (pH 6.0).

synergistic action of PB-Au composite and Pt-NCs, since they both had an ability to catalyze the reduction of H_2O_2 and promote the electron transfer between GOD and the underlying electrode.

3.5. Apparent Michaelis–Menten constant (K_m)

The apparent Michaelis–Menten constant (K_m), which is a critical parameter to describe the enzyme-substrate kinetics of the biosensor, can be obtained from the electrochemical version of the Lineweaver–Burk equation:

$$\frac{1}{I_{ss}} = \frac{K_m}{I_{max}} \times \left(\frac{1}{c}\right) + \frac{1}{I_{max}}$$

where I_{ss} is the steady-state current after the addition of the substrate, c is the bulk concentration of the substrate and I_{max} is the maximum current measured under saturated substrate condition. The K_m value was determined by analysis of the slope and intercept for the plot of the reciprocals of the steady state current versus glucose concentration. The K_m value of the GOD was calculated to be 1.66 mM, which suggested that the apparent affinity between immobilized glucose oxidase and substrate was higher.

3.6. Reproducibility and stability of the biosensor

The reproducibility of the biosensor was investigated by the measurement of the response currents at the same modified electrode for five times in 60 μM glucose. The relative standard deviation was calculated to be 5.8%. The electrode-to-electrode reproducibility was also examined from the responses in 60 μM glucose among six different electrodes made independently following the same procedure. They showed an acceptable reproducibility with a R.S.D. of 6.2%.

Stability is a basic requirement for fabrication of glucose biosensors. The stability of the Nf/GOD/Pt-NCs/PB-Au/GCE was also examined. Generally, denaturation and loss of enzyme could occur during the storage of the biosensor, a result of decreasing the sensitivity. The storage stability of the glucose biosensor was investigated through the response to 35 μM glucose at −0.15 V in 0.1 M KNO_3 (pH 6.0) every 2 days. When not in use, it was stored at 4 °C in a refrigerator. The results revealed that the steady-state response current of the electrode remained relatively constant after 2 weeks and a gradual decrease till a final loss of 20% of the initial response current was observed after 1 month. Such good stability of the biosensor may be attributed to the aspect that the Pt-NCs/PB-Au matrix was stable. The long lifetime of the GOD on the nanoparticles suggested that immobilization of the glucose oxidase on nanoparticles stabilized the enzyme activities.

3.7. Anti-interference of the biosensor

The number of interfering species depends on the working potential and the nature of sample. Such a low-working potential of −0.15 V reduces the responses of common interferences from redox-active species that are usually present in physiological samples and improves the selectivity of the glucose biosensor. The interference test of the glucose biosensor was carried out in 0.1 M KNO_3 (pH 6.0) at −0.15 V in the presence of 70 μM acetum acid, 70 μM uric acid, or 70 μM arginine. The currents generated from the interfering species were negligible to the response current of 70 μM glucose, indicating the interference-free determination of

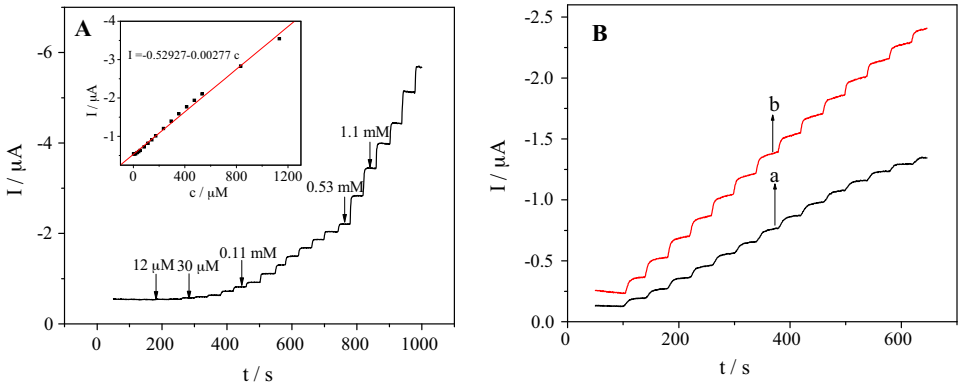

Fig. 6. (A) Amperometric detection of glucose with Nf/GOD/Pt-NCs/PB-Au/GCE in 0.1 M, pH 6.0 KNO_3 solution under stirring. Applied potential: −0.15 V. Inset: the catalytic response vs. glucose concentration. (B) Typical current–time response curve for successive addition of 30 μM glucose obtained by Nf/GOD/PB-Au/GCE (a) and Nf/GOD/Pt-NCs/PB-Au/GCE (b) in stirring 0.1 M KNO_3 of pH 6.0 at applied potential −0.15 V.

Table 1
The comparison of the performance of present biosensor and others reported in the literatures for glucose detection.

Electrode fabrication	Linearity range	Detection limit	Sensitivity	K_m	Ref.
CS/Fe_xO_y–MWCNTs/Pt/GOD/Nf	6.0×10^{-6}–6.2×10^{-3} M	2.0×10^{-6} M	–	9.0 mM	[16]
PB/GOD/silica sol–gel	0–4.75 mM	2.0×10^{-5} M	1.182 mA M^{-1}	6.7 mM	[20]
Fe_3O_4/PB/GOD	5.0×10^{-7}–8.0×10^{-5} M	1.0×10^{-7} M	–	1.44×10^{-2} mM	[21]
CS/CS-PB/GOD	2×10^{-6}–4×10^{-4} M	3.97×10^{-7} M	–	3.73 mM	[29]
Pt/PB/GA-GOD	5×10^{-6}–1.1×10^{-3} M	5×10^{-6} M	43 mA M^{-1} cm^{-2}	6.3 ± 1.2 mM	[30]
PANI–PB/MWNTs/GOD/Nafion	1–11 mM	1.0×10^{-5} M	15.36 mA M^{-1} cm^{-2}	5.1 mM	[38]
Au NPs–PANI/GOD/Nf	1.0×10^{-6}–8.0×10^{-4} M	5.0×10^{-7} M	2.3 mA M^{-1}	–	[39]
PB-Au/Pt-NCs/GOD/Nf	3.0×10^{-6}–1.1×10^{-3} M	1.0×10^{-6} M	2.77 mA M^{-1}	1.6 mM	This work

CS, chitosan; Fe_xO_y–MWCNTs, iron oxide–multiwall carbon nanotubes; GA-GOD, glutaraldehyde-glucose oxidase; PANI–PB, polyaniline–Prussian Blue; MWNTs, multi-walled carbon nanotubes; Au NPs–PANI, Au nanoparticles–polyaniline; –, not available.

glucose at proposed biosensor. Obviously, the higher selectivity of the biosensor was attributed to the contribution of a low operating potential and Nafion coverage, and the efficient and selective mediation by PB.

3.8. The comparison with other glucose biosensors

For comparison, the analytical performance of the proposed biosensor and some other glucose biosensors were listed in Table 1. The information includes the range of linearity, the limit of detection, the sensitivity, the apparent Michaelis–Menten Constant (K_m) of the biosensors. A wider linear range was obtained in the proposed biosensor, when compared to the other biosensors [21,29,38,39]. The detection limit was lower than that of the biosensors [20,38]. The biosensor showed a satisfactory sensitivity, which was revealed by the value of 2.77 mA M^{-1}. As shown in Table 1, the value of K_m of the proposed biosensor was lower than other glucose biosensors excepted for the biosensor in the reference [21]. The data in Table 1 revealed that this biosensor exhibited better combination of the wide linear range, low detection limit, high sensitivity and low value of K_m. The main reason results from the fact is that the forming of the PB-Au composite could effectively overcome the shortcomings of the leakage of PB, and the combination of excellent electrocatalytic activity of PB and Pt-NCs toward H_2O_2 reduction can amplify the response signal.

4. Conclusions

The novel PB-Au nano-composite films were prepared and its integration with Pt-NCs was used to fabricate an electrochemical biosensor for glucose detection. With PB as the electron-transfer mediator, the PB-Au/Pt-NCs/GOD films electrode showed excellent electro-catalytic activity and operational stability toward glucose. The simplicity in fabrication, ease of the detection, high sensitivity, and good reproducibility of the biosensor offer a good promise for practical glucose analysis in real biological systems. It is highly anticipated for the novel PB-Au/Pt-NCs films to be applied in the various glucose assay-based biosensors.

Acknowledgments

This work was supported by the National Natural Science Foundation of China (20675064), Key Lab of Chongqing Modern Analytical Chemistry, the Doctor Foundation of Southwest University (SWUB2008048) and the Fundamental Research Funds for the Central Universities (XDJK2009B013 and XDJK2009C082).

References

[1] J.E. Parkm, M. Atobe, T. Fuchigami, Electrochim. Acta 51 (2005) 849–854.
[2] K. Bandyopadhyay, V. Patil, K. Vijayamohanan, Langmuir 13 (1997) 5244–5248.
[3] S.L. Horswell, C.J. Kiely, I.A. O'Neil, D.J. Schiffrin, J. Am. Chem. Soc. 121 (1999) 5573–5574.
[4] S. Wu, Y.Y. Liu, J. Wu, H.X. Ju, Electrochem. Commun. 10 (2008) 397–401.
[5] D. Feng, F. Wang, Z.L. Chen, Sens. Actuators B: Chem. 138 (2009) 539–544.
[6] X. Wang, C.G. Hu, H. Liu, G.J. Du, X.S. He, Y. Xi, Sens. Actuators B: Chem. 144 (2010) 220–225.
[7] X.H. Kang, Z.B. Mai, X.Y. Zou, P.X. Cai, J.Y. Mo, Anal. Biochem. 369 (2007) 71–79.
[8] Y. Ivanov, I. Marinov, K. Gabrovska, N. Dimcheva, T. Godjevargova, J. Mol. Catal. B: Enzym. 63 (2010) 141–148.
[9] H. Bonnemann, N. Waldofner, H.G. Haubold, T. Vad, Chem. Mater. 14 (2002) 1115–1120.
[10] M.S. El-Deab, T. Ohsaka, Electroanal. Chem. 553 (2003) 107–115.
[11] S. Mandal, D. Roy, R.V. Chaudhari, M. Sastry, Chem. Mater. 16 (2004) 3714–3724.
[12] I. Marinov, Y. Ivanov, K. Gabrovska, T. Godjevargova, J. Mol. Catal. B: Enzym. 62 (2010) 67–75.
[13] H.F. Cui, J.S. Ye, W.D. Zhang, J. Wang, F.S. Sheu, J. Electroanal. Chem. 577 (2005) 295–302.
[14] S.L. Horswell, I.A. O'Neil, D.J. Schiffrin, Phys. Chem. Glasses B 105 (2001) 941–947.
[15] J.S. Ye, A. Ottova, H.T. Tien, F.S. Sheu, Bioelectrochemistry 59 (2003) 65–72.
[16] J.J. Li, R. Yuan, Y.Q. Chai, X. Che, J. Mol. Catal. B: Enzym. 66 (2010) 8–14.
[17] J. Li, X.Q. Lin, Microchem. J. 87 (2007) 41–46.
[18] A.A. Karyakin, Electroanalysis 13 (2001) 813–819.
[19] A.A. Karyakin, E.E. Karyakina, L. Gorton, Anal. Chem. 72 (2000) 1720–1723.
[20] T. Li, Z.H. Yao, L. Ding, Sens. Actuators B: Chem. 101 (2004) 155–160.
[21] J.P. Li, X.P. Wei, Y.H. Yuan, Sens. Actuators B: Chem. 139 (2009) 400–406.
[22] A. Ahmadalinezhad, A.K.M. Kafi, A. Chen, Electrochem. Commun. 11 (2009) 2048–2051.
[23] Q. Zhang, L. Zhang, J.H. Li, Electrochim. Acta 53 (2008) 3050–3055.
[24] M.P. O'Halloran, M. Pravda, G.G. Guilbault, Talanta 55 (2001) 605–611.
[25] R. Garjonyte, A. Malinauskas, Sens. Actuators B: Chem. 56 (1999) 93–97.
[26] A. Malinauskas, R. Araminaite, Mater. Sci. Eng. C 24 (2004) 513–519.
[27] J. Zhang, W. Yang, H. Zhu, J. Li, F. Yang, B.L. Zhang, X.R. Yang, J. Colloid Interface Sci. 338 (2009) 319–324.
[28] S.S. Kumar, J. Joseph, P.K. Lakshminarasimha, Chem. Mater. 19 (2007) 4722–4730.
[29] X.Y. Wang, H.F. Gua, F. Yin, Y.F. Tu, Biosens. Bioelectron. 24 (2009) 1527–1530.
[30] Y. Liu, Z.Y. Chu, Y.N. Zhang, W.Q. Jin, Electrochim. Acta 54 (2009) 7490–7494.
[31] B. Haghighi, H. Hamidi, L. Gorton, Sens. Actuators B: Chem. 147 (2010) 270–276.
[32] Y. Wang, J.W. Ren, K. Deng, L.L. Gui, Q.Y. Tang, Chem. Mater. 12 (2000) 1622–1627.
[33] F. Ricci, G. Palleschi, Biosens. Bioelectron. 21 (2005) 389–407.
[34] D. Zhang, K. Zhang, Y.L. Yao, X.H. Xia, H.Y. Chen, Langmuir 20 (2004) 7303–7307.
[35] M. Ferreira, P.A. Fiorito, O.N. Oliveira Jr., S.I.C.D. Torresi, Biosens. Bioelectron. 19 (2004) 1611–1615.
[36] L. Li, Q.L. Sheng, J.B. Zheng, H.F. Zhang, Bioelectrochemistry 74 (2008) 170–175.
[37] L.D. Zhu, J.L. Zhai, Y.G. Guo, C.Y. Tian, R.L. Yang, Electroanalysis 18 (2006) 1842–1846.
[38] Y.J. Zou, L.X. Sun, F. Xu, Biosens. Bioelectron. 22 (2007) 2669–2674.
[39] Y.Z. Xian, Y. Hu, F. Liu, Y. Xian, H.T. Wang, L.T. Jin, Biosens. Bioelectron. 21 (2006) 1996–2000.